

Department of Physics, Chemistry and Biology

Master's Thesis

Optical properties of free-standing cubic silicon carbide

Mattias Jansson

Linköping, June 4, 2015

LiTH-IFM-A-EX--15/3100--SE



Linköping University
INSTITUTE OF TECHNOLOGY

Department of Physics, Chemistry and Biology
Linköping University
SE-581 83 Linköping, Sweden

Optical properties of free-standing cubic silicon carbide

Mattias Jansson

Linköping, June 4, 2015

Supervisor: **Jianwu Sun**
 IFM, Linköping University

Examiner: **Mikael Syvajarvi**
 IFM, Linköping University



Avdelning, Institution
Division, Department

Semiconductor physics
Department of Physics, Chemistry and Biology
SE-581 83 Linköping

Datum
Date

2015-06-04

Språk

Language

- Svenska/Swedish
 Engelska/English

Rapporttyp

- Report category
 Licentiatavhandling
 Examensarbete
 C-uppsats
 D-uppsats
 Övrig rapport

ISBN

ISRN

LiTH-IFM-A-EX-15/3100--SE

Serietitel och serienummer

Title of series, numbering

ISSN

URL för elektronisk version

<http://urn.kb.se/resolve?urn=urn:nbn:se:liu:diva-XXXXXX>

Titel

Optiska egenskaper för fristående kubisk kiselkarbid

Title

Optical properties of free-standing cubic silicon carbide

Författare

Mattias Jansson

Author

Sammanfattning

Abstract

If your thesis is written in English, the primary abstract would go here while the Swedish abstract would be optional.

Nyckelord

Keywords semiconductor, silicon carbide, SiC, photovoltaic, water splitting, sublimation

Abstract

If your thesis is written in English, the primary abstract would go here while the Swedish abstract would be optional.

Contents

1	Introduction	1
2	An introduction to silicon carbide	3
2.1	Crystal structure	3
2.2	Band structure	4
2.3	Doping in 3C-SiC	7
2.3.1	Donors	7
2.3.2	Acceptors	8
3	Growth technique	11
3.1	About sublimation and nucleation	12
3.2	The sublimation growth setup	14
3.2.1	Doping using sublimation growth	15
4	Characterization techniques	17
4.1	Absorption measurements	17
4.2	Photoluminescence spectroscopy	18
4.3	Nomarski interference contrast microscopy	20
5	Experimental setup	23
5.1	Growth and sample preparation	23
5.2	Characterization experiments	24
6	Results	25
6.1	On seed growth	25
6.2	On B-doped samples	27
7	Discussion	33
7.1	On seed growth	33
7.2	On B-doped samples	34
8	Conclusion	37
9	Future work	39

1

Introduction

SiC is a semiconductor which has attracted interest in research and industry since the 19:th century, when it was first fabricated and used as an abrasive [1]. SiC has been found to be a very stable material. It exhibits a high chemical inertness [2], and is currently commonly used in high power, temperature and radiation applications due to its ability to survive in such environments [3].

SiC is a material which exists in a large number of different polytypes, the most common of which are hexagonal, cubic and rhombohedral. The work described in this thesis deals with the only cubic polytype, denoted 3C. This is one of the structurally most simple polytypes. Compared to the hexagonal counterparts 4H- and 6H-SiC, the 3C-SiC polytype has for a long time been difficult to fabricate in good quality and large volume, and is therefore less studied than the hexagonal types. Recently a method of fabricating good quality free standing material using sublimation growth has been reported [4]. The method has been used to grow the samples used in the work described in this thesis. With this method it is possible to grow free standing 3C-SiC, which means that the material is thick enough to exist as a free standing layer after mechanically polishing away the 4H-SiC substrate.

Cubic SiC has many interesting material properties. It has a higher electron mobility compared to the common hexagonal polytypes. It has also attracted attention as a transistor material, due to low number of interface defects. One application for which 3C-SiC is well suited is the use of boron doped 3C-SiC in an intermediate band photovoltaic solar cell. This is suitable for 3C-SiC due to its band gap size together with the binding energy of boron as an acceptor in the material, which is almost ideal for photovoltaic cell material. This would give a significant increase in photovoltaic cell efficiency compared to the conventional single junction alternative [5][Current efficiencies citation needed]. Another proposed application of 3C-SiC is as a photo-electrode in a photoelectrochemical cell used for water splitting [6, 7], where solar energy is used in the decomposition of water into hydrogen and oxygen gas.

This thesis describes the growth and optical characterization of free standing cu-

bic silicon carbide (*SiC*). The focus is on characterization of the optical properties of 3C-SiC. This is done using absorption spectroscopy, photoluminescence spectroscopy, Chapter 2 gives an introduction to silicon carbide, its structure and properties. Chapter 3 describes the process of growing the material. Both growth of undoped and boron doped material is described here. In chapter 4 a description of the different characterization methods is given, together with a theoretical description of what the measurements can tell about material properties. Chapter ?? describes how the experiments were done and chapter 6 describes the results obtained from the experiments. The results are discussed in chapter 7. Chapters 8 and 9 discuss what has been learned about the material and how the work should be continued in the future.

2

An introduction to silicon carbide

This chapter describes the properties of SiC which are relevant to this thesis. Section 2.1 describes the atomic arrangement in the material, and some different arrangements are discussed. Section 2.2 discusses the energy band structure of 3C-SiC. Finally section 2.3 describes the mechanism and some effects of doping in 3C-SiC.

2.1 Crystal structure

Silicon carbide is a crystalline material consisting of silicon and carbon atoms. The crystalline nature of the material means that the atoms are arranged in a periodically repeating structure called a *lattice*. For given chemical elements there may be several different ways to arrange the atoms in a lattice, i.e. different chemical compounds of the same types of atoms. This is called *polytypism*, where the different lattice structures are called *polytypes* of the material. SiC has a large number of different polytypes - there are more than 250 known polytypes of SiC [8]. The different polytypes can be described as different stacking orders of layers of atoms [9]. Figure 2.1 shows one such layer. The depicted layer is the (111) surface. Here each circle symbolizes one carbon and one silicon atom, displaced a small distance from each other. This pair of atoms is called the *base* of the crystal.

The marked hexagon in figure 2.1 marks an area of the crystal plane which can be used to define the different polytypes, where the polytypes are defined by the placement of the base atoms in this area in different layers. Figure 2.2 shows these stacking sequences for three of the most common polytypes. The depicted orders of the layers refers to one period in the periodic structure. The names for the different polytypes are stated at the top of the figure. The digit in the name refers to the number of layers of a period and the letter denotes the crystal symmetry. The letter *H* denotes the hexagonal polytypes, whereas *C* stands for the cubic polytype. Another common polytype is the 6H-SiC, which thus is a hexagonal structure with a period of

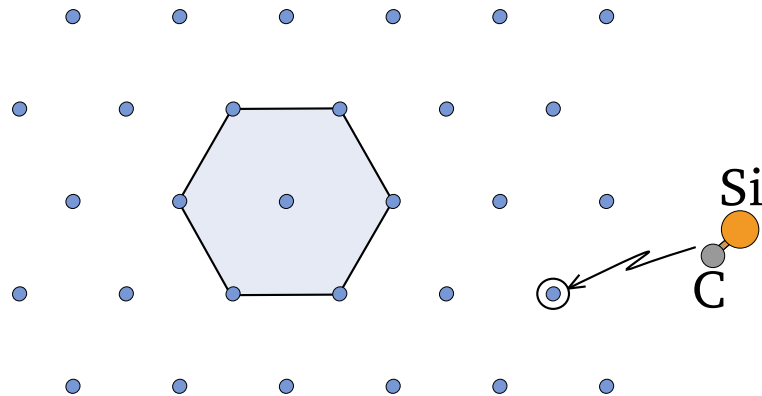


Figure 2.1: Atomic arrangement of the atoms in each (111) layer. Here each sphere corresponds to one carbon and one silicon atom, as shown by the arrow.

six base layers. It should be noted that the 2H-SiC structure is the wurtzite structure and the 3C-SiC is the zincblende structure. The unit cell of the zincblende, or 3C-SiC, crystal has a lattice constant of $a = 4.35 \text{ \AA}$ [10].

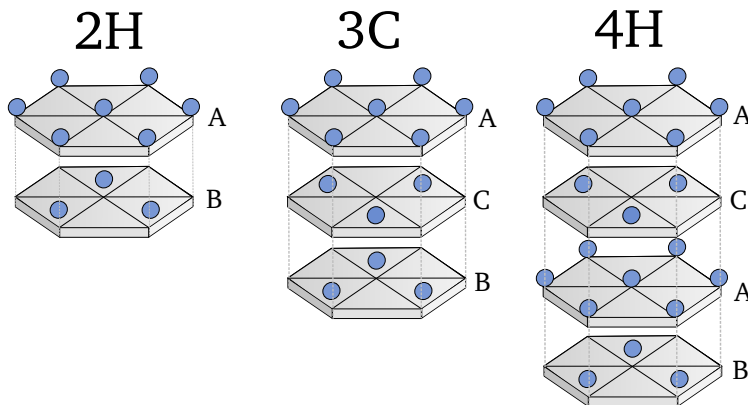


Figure 2.2: Stacking order for the three most simple polytypes.

2.2 Band structure

In SiC the atoms are bonded together with covalent bonds [Citation Zumdahl: Chemistry?] into a crystal. When the atoms are bonded together, the energy levels for the electrons in the material are defined by the material and lattice structure. This means that all materials have characteristic energy levels. When many atoms are bound together, as is the case in crystals, the discrete energy levels for the electrons in the atoms merge together to form continuous bands, called energy bands.

The band structure for 3C-SiC is shown as a band diagram in figure 2.3. In this figure, each curve describes allowed energies for the electrons, and the spaces in between the curves are not allowed. The x-axis shows different points in reciprocal space, or k -space. The marked points are specific points in the first Brillouin zone of k -space, and the intermediate intervals form straight lines between the points. This figure has been obtained using the approximate method of pseudopotentials, as described in [11]. Here the zero point energy has been chosen to be at the Γ -point in k -space.

The grayed area in the figure is the *band gap* of the material, since there are no allowed electronic states in this area. The band with lower energy than the band gap is called the valence band, and the band with higher energy is called the conduction band. 3C-SiC, as is characteristic for semiconductors, has the Fermi level in the middle of the band gap. This means that at the temperature of 0 K, all electrons will be in the valence band, and the conduction band will be unoccupied. When the conduction band is unoccupied the material will not be able to conduct electricity. If the temperature is raised above 0 K there will be some occupation of the conduction band and some electrical conduction will be able to occur. With a higher temperature there will be more electrons in the conduction band and thus a higher conductivity of the material.

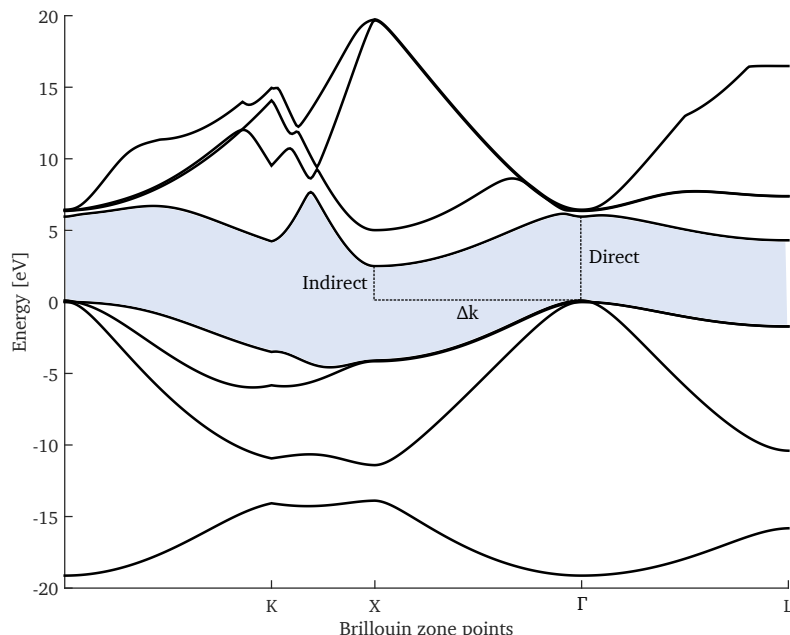


Figure 2.3: The band diagram of SiC at ambient conditions for different positions in the Brillouin zone. The indirect and direct band gaps are marked in the figure. The marked area is the band gap. The energy levels have been obtained using the pseudopotential method, as described in [11].

In the figure 2.3 it can be seen that the smallest energy difference between the valence and conduction bands is between the Γ -point in the valence band and the X-point in the conduction band. This difference is called the *band gap*. The difference between the Γ - and X-points is called the indirect band gap, while the difference between the values at the Γ -point is called the direct band gap, as illustrated in the figure. These values are given in table 2.1. The value for the indirect band gap at room temperature is taken from the simulation, whereas the latter values are taken from literature.

Table 2.1: Values for the indirect and direct band gap energies. The indirect values are given both for room temperature and low temperature, as this will be of value later in the thesis.

$E_{g,\text{indirect}}$ (300 K)	$E_{g,\text{indirect}}$ (2 K)	$E_{g,\text{direct}}$ (300 K)
2.36 eV	2.42 eV [10]	6.00 eV [12]

When an electron makes the indirect transition from the valence to the conduction band the energy is increased by E_g , and the k-value is changed, as indicated by Δk in figure 2.3. This change of k-value implies a change in momentum of the electron, since k and momentum p is related by

$$p = \hbar k,$$

where \hbar is Dirac's constant. This is of importance when studying interaction between the material and light. Photons are capable of providing the energy needed to transit from the valence to the conduction band, but cannot provide the change of momentum needed. The law of conservation of momentum requires the total momentum of the system to be preserved during the transitions. The extra momentum can however come from interaction with phonons.

The phonon energy spectrum has four ground modes, since there are two different kinds of atoms in the material. There are the acoustic and optical phonon modes. Theoretical calculations of the phonon dispersion curves for 3C-SiC have been done by Karch et al. [13]. They show the four modes: TA, LA, TO, LO, and give the wavelength for each mode. The transition in k-space for the indirect transition is between the Γ - and the X-points, hence it is of interest to know which phonon wavelengths and energies this corresponds to. Table 2.2 shows these computed wavelengths and the corresponding energies, which have been calculated using the fact that

$$E_{\text{meV}} = \frac{hc(\frac{1}{\lambda_{\text{cm}}})}{e} \times 10^5,$$

where h is Planck's constant, c is the speed of light and e is the elementary charge.

Table 2.2: Inverted wavelengths and energies for the Γ -X transition. Values for λ from [13].

Mode	$\lambda^{-1} [\text{cm}^{-1}]$	E [meV]
TA	368	45.6
LA	637	79.0
TO	760	94.3
LO	829	102.9

2.3 Doping in 3C-SiC

Doping is a way to change the electronic structure of a material by substituting some of the native atoms with a foreign element. In the case of SiC this means that either silicon or carbon is replaced by some other element. How the band structure of the material is changed depends on which impurity is introduced to the crystal. By choosing the dopants it is possible to tailor the band structure to create various new properties of the material.

An important factor for how the band structure is changed is the number of valence electrons in the introduced element, compared to the element it replaces. Silicon and carbon both have four valence electrons, creating four bonds to its neighbouring atoms in the crystal. The electrons are strongly bound to the atomic nuclei, requiring energy corresponding to the band gap to free one electron. If one silicon or one carbon atom is replaced by an element with five valence electrons however, the additional electron is not as strongly bound to the nucleus and can easily release an electron to the conduction band. This is called a *donor* atom. Similarly if an atom with only three valence electrons is introduced to the crystal, it can readily bind an electron from the valence band, creating an electron deficiency, or *hole* in the valence band. This is called an *acceptor* atom. Figure 2.4 shows a simplified band diagram with a donor and an acceptor level. The donor level donates an electron to the conduction band by supplying the energy E_D to the electron. The acceptor accepts an electron from the valence band by supplying the energy E_A . The energy required to supply the material with one carrier from a dopant level is called the *binding energy* (or *ionization energy*) of the dopant.

2.3.1 Donors

Since silicon and carbon both have four valence electrons, a donor atom in SiC must have five or more electrons. One common donor is nitrogen, which has five valence electrons. This means that each added N-atom can supply the conduction band with one electron. A material with more electron carriers than the hole counterpart is said to be an *n-type* material. Freitas et al. have measured the binding energy of nitrogen in 3C-SiC, and found it to be 54 meV [14]. This means that the lowest N-level is 54 meV below the conduction band.

N-doping can be achieved intentionally by fabricating the material in a nitro-

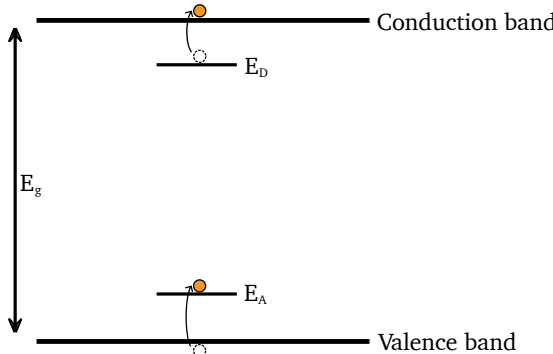


Figure 2.4: Two new energy levels are introduced by doping.

gen atmosphere, but nitrogen always present in sublimation grown material even at vacuum conditions with continuous pumping[15]. This means that material grown by this method is generally n-type. The n-type material can also be created by other elements in group five. Reports of doping with As, P and Sb exist, but are far less common than N-doping [16].

2.3.2 Acceptors

Acceptor atoms need to have fewer valence electrons than silicon and carbon, which is why group three elements are the most common. These include boron, gallium and aluminum, which have the binding energies 257 meV [14] and 735 meV [5] respectively. A material with more acceptors than donors is said to be *p-type*. Table 2.3 summarizes the different dopant energy levels.

Table 2.3: Binding energies for some of the most common SiC dopants.

Element	Dopant type	$E_{D/A}$ [meV]	Reference
N	Donor	57	[14]
B	Acceptor	735	[5]
Al	Acceptor	257	[14]

The B-doping energy level is of particular interest for photovoltaic applications, where the binding energy is ideal for the intermediate band photovoltaic solar cell. This is described in more detail in chapter ??.

There are several ways to create doped materials. It can be done by ion implantation, where ions are accelerated to high energies and then made to collide with the undoped material [16]. It can also be done as the material is grown, by including the doping element in the ambient. The first method has several advantages: it can be

done with good control over doping density and it is possible to select only certain areas of the material to dope. The latter method is done *in situ*, so it requires no additional equipment. It is also not as prone to create defects as the ion implantation method is, where annealing is often required after implantation in order to reduce the number of defects. In the work described in this thesis, the method of doping is to include the doping material during the growth. This method is described in more detail in chapter 3.

During doping some of the native atoms are replaced. This will have effects on the quality of the produced material. Different elements have different atomic radii, so replacing one atom by one of a different element will create some strain in the material. This may lead to defects in the material.

3

Growth technique

SiC can be fabricated by several different techniques, and the different techniques are advantageous for different polytypes and applications. Some of the most common methods are *sublimation epitaxy*, *liquid phase epitaxy (LPE)*, *chemical vapour deposition (CVD)* and *physical vapour transport (PVT)* [17].

The goal when growing freestanding material is to have high quality material of large enough thickness to allow the substrate and transition layer to be polished away. Up to this point in time, researchers have had more success fabricating high quality 4H-SiC and 6H-SiC material compared to 3C-SiC [3]. The hexagonal polytypes are commonly fabricated using PVT. This method has not been widely adapted to 3C-SiC growth however, which is often attributed to the fact that this method uses homoepitaxy, and there are no 3C-SiC seeds widely available. Nishino et al. reported in 1983 a growth rate of approximately 2.5 microns per hour with the CVD technique for 3C-SiC growth [18]. This rate is much too low to create free standing material. The growth rate for CVD growth has been improved since this time, and in 2002 Nagasawa et al. reported a rate of $40 \mu\text{m/h}$ [19], which makes it possible to fabricate free standing 3C-SiC.

Another growth method is sublimation epitaxy, which was demonstrated by Lely in 1955 [20]. In this method material is transferred between a source material and a substrate using sublimation. Recently there have been reports of high quality cubic SiC fabricated by sublimation growth. Growth rates as high as $500 \mu\text{m/h}$ have been reported using this method, while still growing good quality material [4]. This high growth rate is obviously ideal for growth of free standing (and even bulk) material. This chapter describes in detail the sublimation method in general and more details about the setup used in this work.

3.1 About sublimation and nucleation

Sublimation is the phase transition where a material transitions between solid and gas, without the intermediate liquid phase. At normal conditions SiC does not melt, but rather it sublimes. For SiC to melt a pressure of 100,000 atm and a temperature of at least 3200 °C is required - at atmospheric pressure SiC can only sublime [21]. Sublimation of a SiC source material will give a vapour consisting of different molecules consisting of silicon and carbon, for example Si, Si₂C, SiC₂ etc. The composition and vapour pressure of the gas can be controlled using parameters such as temperature and pressure of the ambient.

If a substrate is placed in the silicon-carbon vapour, some of the material will be adsorbed on the surface of the substrate, in the form of *adatoms*. When many such atoms are adsorbed at the surface they bind together, forming a *nucleus* of crystal growth. In a sublimation growth setup, a source of SiC is heated, initiating the sublimation. The vapour then travels to an appropriate substrate, by the means of a heat gradient. Material is adsorbed on the substrate which forms the grown crystal. Figure 3.1 shows a schematic of this process. The vapour is transported from the source to the substrate against the temperature gradient. The higher temperature is at the source.

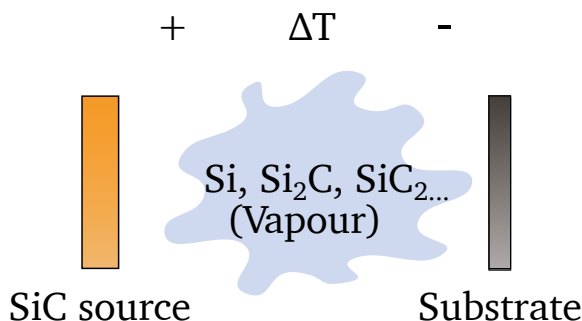


Figure 3.1: A vapour containing silicon and carbon molecules is created by sublimation of a SiC source. The vapour is adsorbed at the substrate.

As the material is adsorbed at the substrate the growth begins. The crystal growth is governed by the free energy of the whole system. A decrease in free energy works to promote the growth. In crystal growth, a decrease in free energy is an increase in chemical potential μ , meaning that crystal growth is driven by an increase in chemical potential. The system is made up by the vapour and the crystal phases, hence a change in chemical potential is given by

$$\Delta\mu = \mu_v - \mu_c,$$

where μ_v is the chemical potential for the vapour and μ_c is for the crystal. For growth from vapour phase, the chemical potential difference between vapour and crystal is dependent on the *partial vapour pressure* and the *equilibrium vapour pressure* through

the formula

$$\Delta\mu = k_B T \log(p/p_e),$$

where p is the partial vapour pressure and p_e is the equilibrium (or saturated) counterpart. Defining the *supersaturation*, σ , as

$$\sigma = \frac{p - p_e}{p_e}$$

thus

$$\Delta\mu = k_B T \log(\sigma + 1).$$

Taking the first order Taylor expansion this becomes

$$\Delta\mu \approx k_B T \sigma.$$

It is concluded that the change in chemical potential is directly proportional to the supersaturation of the system. An increase in supersaturation will hence promote growth and increase growth rate.

Supersaturation is also a measure of how the crystal is formed. SiC can grow in several ways. One such way is called *spiral growth*. In this growth method there are steps which originate from one point on the surface. As atoms attach to these steps, they move around the center point. This gives a spiral shape on the surface. Another way of growth is *2D nucleation*. This is when atoms are adsorbed to a flat surface, and the adatoms bind to each other creating a 2D nucleus on the surface. Additional atoms will attach to this nucleus as they are adsorbed to the surface. The value of supersaturation governs which of these two methods is present.

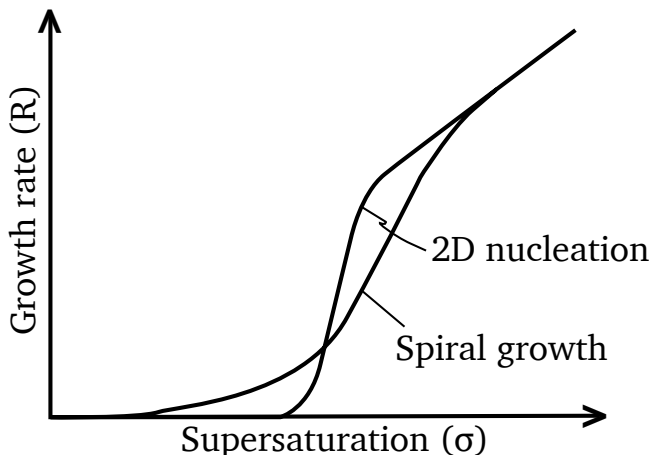


Figure 3.2: The growth rate for different modes vary depending on supersaturation.

Figure 3.2 shows the general relationship between the growth rate (R) and the supersaturation (σ). It should be noted that at a certain value of σ the growth rate

of 2D growth is higher than that of spiral growth. At σ higher than this value the 2D growth will dominate over spiral growth.

The growth model for 3C-SiC on off-axis samples is described in detail by Jokubavicius et al. [4]. The model can be divided into three parts. Initially a large terrace region is formed at one edge of the substrate. The terrace is grown homoepitaxially. On this terrace small areas of 3C-SiC are formed, and will eventually merge. Lastly the 3C-SiC grows from the terrace onto the rest of the substrate, in step flow growth. In step flow growth, the steps inherent in off-axis samples are overgrown with 3C-SiC by enlargement of the steps. This is sometimes also called *lateral enlargement*.

3.2 The sublimation growth setup

The sublimation growth process used in this work is setup as shown in figure 3.3. An insulating graphite foam is placed inside a quartz tube, which is surrounded by a copper coil (shown as a cutaway in the figure). The copper coil is connected to an RF-generator capable of creating a current in the coil. The foam cylinder contains a graphite crucible, which will couple with the magnetic field created by the current in the copper coil. This will heat the crucible. To measure the temperature of the crucible there is a pyrometer fixed above the quartz tube (not shown in the figure), which can measure the temperature of the crucible through a small hole at the top of the insulating foam.

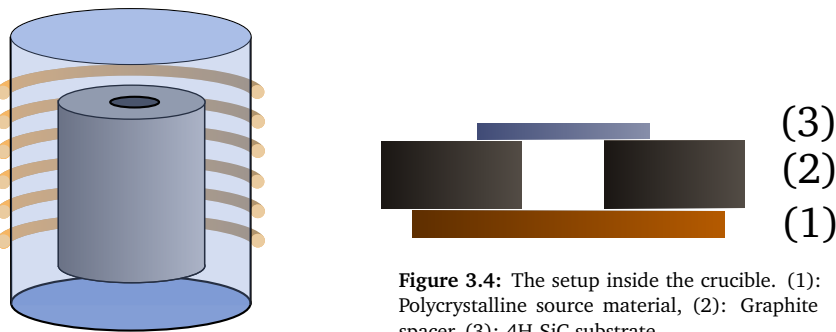


Figure 3.4: The setup inside the crucible. (1): Polycrystalline source material, (2): Graphite spacer, (3): 4H-SiC substrate.

Figure 3.3: An outside view of the reactor setup of the sublimation growth method. A copper coil surrounds a quartz tube containing an insulating graphite foam.

The graphite crucible contains the components of the sublimation process, as shown in figure 3.4. At the bottom of the crucible is a source material, which will sublime away during the growth. When growing free-standing 3C-SiC, a polycrystalline SiC wafer piece is used as source material. The source and the substrate are separated by a graphite spacer, which is a disc with a hole in it where the vapour can flow freely. The size of the spacer and the hole can be varied depending on the desired size of the

grown sample. The substrate can consist of different materials, generally 4H- or 6H-SiC. Wafers if both 4H- and 6H-SiC are commercially available and can thus readily be used as substrates in growth. When the wafers are cut, they can be cut at different angles, i.e. in different crystal planes.

Growing on on-axis substrates will give many nucleation sites. As these sites expand and merge with each other there will be many defects at the interfaces. These defects are called *double positioning boundaries (DPB)*. The off-axis substrates have a surface which contains many shallow steps. As the 3C-SiC has nucleated at the edge of the growth area, the nucleation site will expand laterally along the step-flow direction. This growth method is called *lateral enlargement mechanism*, and is the main principle of 3C-SiC sublimation growth, after nucleation has occurred. The density of DPBs are greatly decreased in this manner. This process is described in detail by Jokubavicius et al. [4].

As described earlier in this chapter, the growth temperature and pressure are vital parameters to determine growth rate and thus also crystal quality. In sublimation growth these parameters can easily be controlled during growth. The temperature is controlled by modulating the current from the RF-generator. A temperature ramp up scheme is used to facilitate proper step flow growth. The growth starts by homoepitaxial spiral growth of 4H-SiC on the substrate, until the supersaturation has become large enough for 2D-growth to occur. This is in accordance with figure 3.2. It has been shown that the temperature window for 3C-SiC growth is rather narrow [22], hence proper control of the temperature is vital for good quality material. The temperature ramp up scheme is done in two or three parts. First the temperature is increased by increasing the power from the RF-generator. This is done in intervals of several minutes per 100 W. As the desired temperature is reached, it is held for the desired amount of time. For some samples a third step is added, where after growth for some time at the first temperature level, it is again increased to a higher level and held there for some additional time. These schemes are sometimes called one and two step temperature schemes respectively.

Another important parameter is the pressure in the reactor during growth. To avoid inclusions of foreign material in the crystal a low pressure during growth is required. Typically a pressure of 10^{-4} to 10^{-5} mbar is used, which is achieved with dynamic vacuum. Some nitrogen inclusions will be unavoidable even at these pressures. A residual N-doping in the order of 10^{16} cm^{-3} has been shown in material grown under these conditions [4], which can be compared to 10^{22} cm^{-3} silicon or carbon atoms in the crystal.

For a good quality crystal to form, the proper ratio between silicon and carbon must be present in the vapour. To avoid the problem with excess of carbon, a *carbon getter material* is often used. This is a material which binds carbon from the vapour, thus reducing the C/Si ratio. One such material is tantalum.

3.2.1 Doping using sublimation growth

It is possible to grow intentionally doped material using the sublimation growth method. To do this, the pure SiC polycrystalline source is exchanged for a doped source with the appropriate dopant density. The vapour from the sublimation will

then contain the dopant element. Figure 3.5 shows the crucible setup for growth of doped material. Here the substrate contains a 3C-SiC seed before the growth starts. This is to facilitate cubic growth.

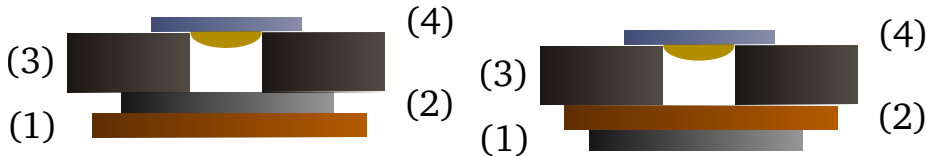


Figure 3.5: The crucible setup when doing doped growth. The source and seed (4) is separated by a graphite spacer (3) from the doped (2) and undoped (1) source material.

Figure 3.6: Indirect growth. Here the doped (1) and undoped (2) source materials have changed places as compared to direct growth.

It is now vital to have the proper ratio between all of the elements in the vapour phase, i.e. silicon, carbon and dopant. In this thesis a new method to possibly alter this ratio is introduced. This method is called *indirect doping*, and is shown in figure 3.6. This differs from the direct doping shown in figure 3.5 in that the doped source is now separated from the substrate by a nominally undoped source layer. If the doped source material is not homogeneous, the indirect method is hoped to give a better grown material, as well as reduce the dopant content in the vapour.

4

Characterization techniques

To investigate the material properties after growth, the samples must be characterized. There are many established techniques to do this. This chapter gives a description of the characterization techniques used to obtain the results in this thesis. This thesis focuses mainly on the optical properties of the grown samples, but the work also includes some morphology studies. The specifics of the experiments performed are given in chapter 5.

4.1 Absorption measurements

Absorption measurements are performed to find how much light is absorbed or transmitted when it hits the sample. In this way the band structure can be found even for samples with little or no luminescence. During measurements, light of different wavelengths hits the sample, some of which is absorbed and some is transmitted. The transmitted light passes through a spectrometer which measures the light intensity as a function of the wavelength. By measuring the light intensity before (I_0) and after (I) the sample, it is possible to compute the logarithm of the ratio of the two, which constitutes the *absorption* of the sample, i.e.

$$A(\lambda) = \log \left(\frac{I_0(\lambda)}{I(\lambda)} \right). \quad (4.1)$$

Generally some wavelengths are absorbed more than others. In semiconductors, light is absorbed to allow electrons to make a transition from a lower to a higher energy level. The band structure determines which transitions are allowed and which are not. Absorption of a certain wavelength means that there is an allowed transition with the same energy. The energy and wavelength relate through the formula

$$E = \frac{hc}{\lambda}, \quad (4.2)$$

where h is Planck's constant and c is the speed of light.

From absorption measurements it is also possible to find the absorption coefficient. This is done by using the Beer-Lambert law of transmission:

$$I = I_0 e^{-\alpha L}. \quad (4.3)$$

Where α is the absorption coefficient and L is the thickness of the sample. Combining this with equation 4.1 we can find the absorption coefficient. This is done by

$$I = I_0 e^{-\alpha L} \implies \log\left(\frac{I_0}{I}\right) = \alpha L \log(e),$$

which gives

$$\alpha = \frac{A}{L \log(e)}. \quad (4.4)$$

Having found the absorption coefficient it is also possible to find the effective band gap from the absorption data. This is done by the means of a *Tauc plot* [23]. In this method, the abscissa and ordinate of a plot contain the quantities hv and \sqrt{ahv} respectively, where v is the frequency of the light. If the data is obtained from an indirect semiconductor performing an allowed electron transition, then a part of the graph will be linear. Extrapolating this linear function to the energy axis will yield the band gap.

4.2 Photoluminescence spectroscopy

Photoluminescence (PL) spectroscopy is a very powerful tool in optical characterization of semiconductors. It is a non-invasive and fast technique. PL is similar to absorption spectroscopy in that a light source is aimed at the sample to induce electron excitations. As an electron radiatively recombines with a hole, a photon is emitted. These emitted photons are called the *luminescence* of the sample, and is what is measured in PL spectroscopy. Figure 4.1 shows a schematic of the method of generating luminescence. As the laser beam (A) hits the sample (B), photoluminescence (C) is generated. As not all laser light is absorbed, some of the light reflects away from the sample (D).

The process of excitation and recombination is shown in figure 4.2, where a photon is captured (a) and generates an *electron hole pair (EHP)* (b). The EHP then recombines and emits a photon of energy corresponding to the band gap, E_g (c).

To generate an EHP by a transition between the valence and conduction bands, the energy of the light must be greater than the band gap. This is in accordance with the principle of conservation of energy. The laser must be chosen accordingly. Not only the energy is conserved in this process, but as is the momentum. Since SiC is an indirect semiconductor (see figure 2.3), an electron moving across the band gap has a change in momentum. The light momentum is far too small to compensate for this change. To allow the EHP to be generated, the change in momentum is contributed by phonons. As the transition occurs, a phonon is either created or annihilated. The phonon energies for the different modes in 3C-SiC are described in section 2.2. The

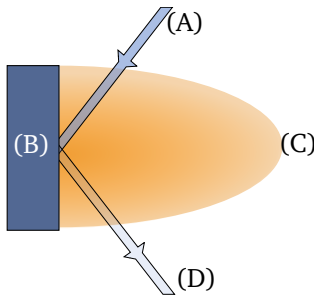


Figure 4.1: Photoluminescence induced from a sample by a laser beam.

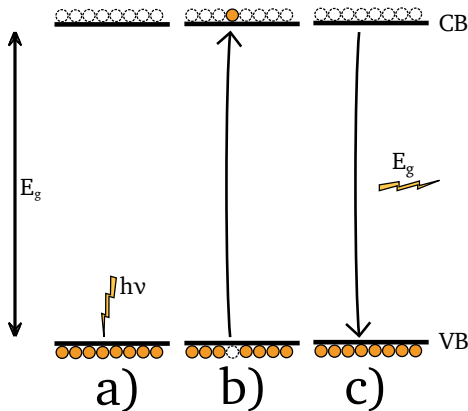


Figure 4.2: An EHP is generated by capture of a photon with energy $h\nu$ (a), (b). The EHP recombines to emit a photon of energy E_g .

phonons show in PL spectra as lines with energies slightly smaller than the value of the actual energy transition, called the *zero phonon line* (*ZPL*). The phonon lines are called *phonon replicas*.

The phonon replica lines can be used to investigate the biaxial stress in the material. The PL intensity of the transverse optical and longitudinal acoustic modes should be the same if the material is without internal stress. Hence the ratio

$$\frac{I_{LA}}{I_{TO}}$$

should be near unity in good quality samples [15]. Here I_{LA} and I_{TO} are PL intensities of arbitrary units. The phonon lines can also be used to estimate the doping concentration of a dopant. Camassel et al. have introduced a method where the full width at half maximum (FWHM) value of the TA-line is used for this purpose.

If doping levels are introduced in the band structure, then transitions can occur between such levels and the bands. In this case there will be another set of ZPL and phonon replicas at the new transition energy. The band structure can thus be inferred

from the PL spectrum.

As the EHP are generated, the electron and hole will interact with each other through the Coulomb force if they are near enough to each other. Due to their charge difference, they will start to orbit each other. This is called the *exciton* quasiparticle. The energy of recombination of an exciton is slightly shifted from a normal recombination of a EHP due to the potential energy from the Coulomb interaction. At room temperature the thermal energy from the ambient is generally high enough to split the exciton into a free electron and hole, so the excitons are not seen in the PL spectrum. At very low temperatures there is not enough energy to split the exciton, so the PL spectrum shows this shift in the recombination energy attributed to the Coulomb interaction. Some excitons can freely move in the sample, but some excitons bind to impurities in the sample. There is a small energy difference in the free and bound excitons attributed to the binding energy to the impurity. It is thus possible to distinguish from the free and bound excitons in the PL spectrum. They show that the concentration of nitrogen donors in the sample is proportional to the FWHM, Γ , through the formula

$$\Gamma_{\text{TA}} = A[N]^{1/n}. \quad (4.5)$$

Here A and n are constants and [N] denotes the concentration on nitrogen donors. This method has however not been validated for acceptor type impurities.

The PL setup can be described as follows. An optical setup is used to focus a laser beam on a sample. The emitted photoluminescence passes through another optical setup and is focused into a spectrometer. The spectrometer separates the incident light by wavelength, generally by the use of a grating. Photons with a given wavelength can now be collected by a photomultiplier tube or a CCD camera, and the photon intensity for the wavelength spectrum can be computed. Light is captured during a set time (generally ranging between seconds to minutes depending on the sample and setup).

The sample can be placed in a cryostat to measure the luminescence at low temperature, or measurements can be performed in room temperature. Various types of cryostats exist, generally using either liquid nitrogen or helium. In this work results have been obtained using room temperature measurements and by the use of a liquid helium cryostat.

4.3 Nomarski interference contrast microscopy

Nomarski interference contrast microscopy, also known as differential interference contrast microscopy, is a version of an optical microscope designed to be able to investigate the inside of samples. The method utilizes the polarization of light to give slightly different light paths depending on where in the sample the light passes. The setup is shown in figure 4.3.

The light is initially unpolarized. After passing a 45° polarization filter, the light enters a Wollaston prism. This prism will split the light in different directions depending on the polarization, creating two diverging beams. One beam will have light polarized in 0° direction and the other in the 90° direction. These two beams are focused on the sample by a lens, but made to hit the sample at slightly different

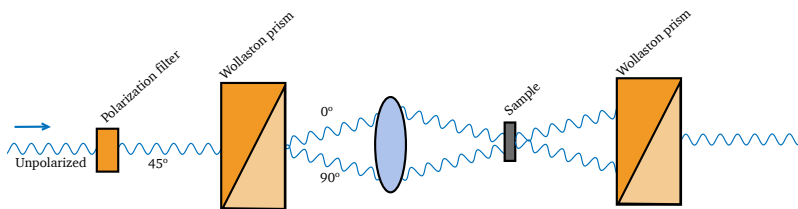


Figure 4.3: A schematic of the Nomarski microscope setup. The light passes through the setup from the left to the right.

positions. This will give the light beams slightly different paths through the sample. As the beams leave the sample they will enter another Wollaston prism, which will merge the two beams into one, and give the beams the same polarization, 135° . If the beams have travelled different lengths in the sample, or if the sample composition has varied between the two paths, then the beams will be slightly out of phase. This phase difference will lead through interference between the beams lead to optical contrast.

One possible use for the Nomarski microscope is to detect different thickness in the sample. It can also be used to detect different sample composition, if the compositions have different refractive indexes. As an example if a 3C-SiC sample has hexagonal inclusions, then these will give contrast in the microscope since the hexagonal and cubic polytypes have different refractive indexes.

5

Experimental setup

In this chapter, the experimental setup details are explained. The chapter is divided into two parts. The first part describes how the samples were grown and prepared. The second part describes details on the experimental setups for the characterization experiments.

5.1 Growth and sample preparation

All samples used in this work are grown using sublimation growth, as described in section 3.2. The nominally undoped samples are grown using two layers of XXX mm thick polycrystalline SiC source material. 4H-SiC substrates with 4° off axis surface were used for undoped growth. The substrates were chemically cleaned before growth. Both the carbon and the silicon face of the 4H-SiC substrates were used during growth of undoped samples.

The doped samples were grown using either direct or indirect doping methods, as described in section 3.2.1. The source material for doped growth was doped polycrystalline SiC, doped with boron concentrations of 10^{18} , 10^{19} or 10^{20} cm⁻³. This was used together with a piece of undoped source material. The doped samples were grown either homoepitaxially on an unintentionally doped seed, or heteroepitaxially on the silicon face of a 4H-SiC 4° off-axis substrate.

A piece of tantalum foil was placed in the bottom of the crucible for use as a carbon getter during growth of all samples. The source and substrate or seed were separated by a 1 mm thick graphite spacer for all samples. The substrate was held in place on the spacer by a graphite plate placed on top. All samples were grown at pressures in the order of 10^{-4} to 10^{-5} mbar, varying during the growth process. A vacuum pump was connected to the reactor and running continuously during growth. The temperature and growth time were varied between samples, and are given for individual samples in section 6. The temperature was changed by varying the power

supplied by the RF generator to the copper coil. The reactor setup is described further in section 3.2. Care was taken to place the insulating foam containing the crucible in the same position in the reactor for each run.

After growth the reactor was cooled in vacuum, by instantly setting the RF-generator to 0 W when the growth time was over. Cooling time was reduced by the use of a fan placed outside of the reactor. Optical microscopy images were done on samples as grown, but any other characterization was done after chemically cleaning the samples.

5.2 Characterization experiments

The absorption measurements were done with a PerkinElmer Lambda 950 UV/VIS setup. The software used was PerkinElmer UV WINLAB for molecular spectroscopy. Measurements were done in the range between 2000 to 350 nm. Samples were mounted on a black cardboard piece with a hole for light to pass through. Two hole sizes were used: 3 mm and 4 mm in diameter. Most samples were measured after mechanical polishing of the substrate, i.e. free-standing, but some samples were measured with the substrate remaining. The wavelength step length of the spectrometer was 5 nm.

Low temperature photoluminescence measurements were performed using a liquid helium cryostat. The helium was supercooled to 2.6 K using a pump. The wavelength resolution of the setup was 0.25 Å. A laser of wavelength 351 was used.

6

Results

In this chapter, the results of the experiments are shown. The chapter is divided into two parts. The first part shows the results for unintentionally doped seed growth, whereas the second part shows the results of B-doped samples. The results are further discussed in chapter 7.

6.1 On seed growth

This section contains the results of characterization of unintentionally doped 3C-SiC seeds. To investigate growth of seeds to be used for B-doping, seeds were grown on both carbon and silicon face of the 4H-SiC. Table 6.1 shows the growth conditions and properties of the seeds grown on carbon face. The sample thickness is excluding the substrate thickness. Terrace coverage indicates the percentage of the step flow terrace covered by 3C-SiC rather than any other polytype. Not all sample coverages were measured quantitatively, but the percentages in the table are after initial examination of micrographs of the other samples thought to be representative. The silicon face seeds were all grown at temperatures 1850/1925 °C during times of 0:30/1:00 (hours/minutes). Nine out of ten of the silicon face grown seeds had a terrace coverage of 100 %, whereas none of the carbon face samples had complete terrace coverage. The terrace coverage was estimated from optical micrographs.

Figures 6.1 and 6.2 show representative micrographs of the terrace of carbon face grown seed S5. Figure 6.1 shows a reflection mode micrograph. It can clearly be seen that there are a few large areas of different polytypes. The hexagonal polytype regions show spiral growth, which on carbon face 4H-SiC manifests as a star shape. The 3C-SiC regions look smoother, and show some of the characteristic triangle shapes. Figure 6.2 shows a Nomarski mode micrograph, showing clear contrast between the different polytype regions.

Figure 6.3 shows a reflection mode silicon face grown seed. On this sample the

Table 6.1: Growth conditions of seeds of undoped 3C-SiC grown on the carbon face of the substrate. For samples grown using a two stage temperature ramp up, the temperatures and growth times for each step are both shown.

	Temperature [°C]	Time [h:min]	Sample thickness [μm]	Terrace coverage [%]
S1	1825	4:00	700	40
S2	1850/1925	0:30/1:00	800	20
S3	1850/1925	0:30/1:00	800	
S4	1850/1925	0:30/1:00	900	30
S5	1875/1925	0:15/1:00	800	50
S6	1925	1:00	700	20
S7	1925	1:00	700	

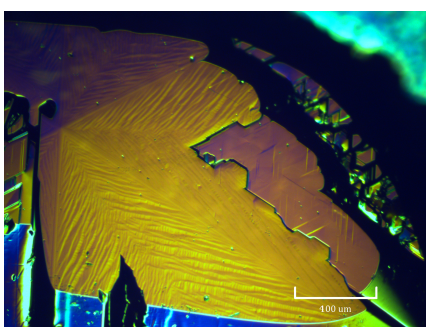


Figure 6.1: Reflection mode micrograph of the facet of C-face seed S5.

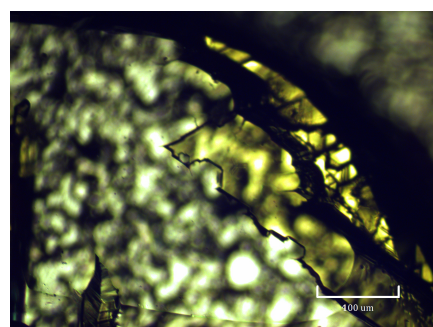


Figure 6.2: Nomarski transmission mode micrograph of the facet of C-face seed S5.

whole facet is covered with the 3C-SiC polytype. This micrograph is representative of the Si-face grown seeds, most of which had complete facet coverage.

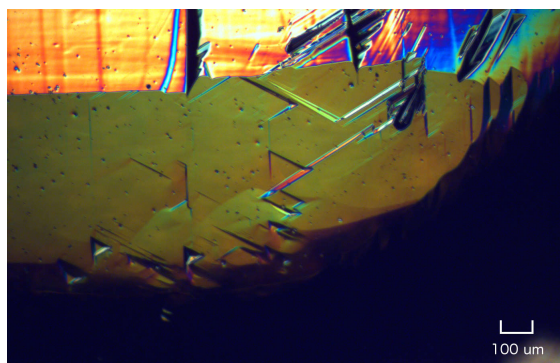


Figure 6.3: Reflection mode micrograph of the facet of a Si-face seed.

6.2 On B-doped samples

This section shows the results of characterization of B-doped samples. Table 6.2 shows the growth conditions and sample thickness of the grown B-doped samples. The thickness is measured for the doped layer, excluding both the substrate and the undoped seed. The growth mode is the stacking order of the doped and undoped source materials in the crucible, as described in section 3.2.1. The *Seed* column displays whether the sample was grown on a 3C-SiC seed or on a 4H-SiC 4° off-axis substrate. All substrates used for B-doped samples are Si-face, and the seeds are all grown on Si-face.

Table 6.2: Growth conditions of the doped samples are shown in this table. The growth mode describes which samples are grown using direct or indirect doping methods. These methods are described in section 3.2.1. The doping concentration is given for the source material.

	Temp. [°C]	Time [h:min]	Thickness [μm]	Doping [cm ⁻³]	Mode	Seed
D1	X	X:XX	X	10 ¹⁸	Direct	Yes
D2	1825	2:30	350	10 ¹⁸	Direct	Yes
D3	1825	3:00	360	10 ¹⁸	Direct	Yes
D4	X	X:XX	440	10 ¹⁹	Direct	Yes
D5	1825	2:30	320	10 ¹⁹	Direct	Yes
D6	X	X:XX	X	10 ²⁰	Direct	Yes
D7	1825	2:30	220	10 ²⁰	Direct	Yes
D8	1825	2:30	380	10 ¹⁸	Indirect	Yes
D9	1825	2:30	380	10 ²⁰	Indirect	No

Figure 6.4 shows the surface morphology of an undoped sample (a), doped sample number D1 (b), doped sample number D4 (c) and doped sample number D6 (d). It is clearly seen that the undoped sample has a better crystal quality compared to (b) and (c), but (d) which is grown with a highly doped source shows good crystal quality. The micrographs are representative for the whole surface morphology of the samples. It should be noted that the samples (b)-(d) are grown using a source material doped with dopant concentration of 10¹⁸, 10¹⁹ and 10²⁰ cm⁻³ respectively.

Figure 6.5 shows micrographs of samples D1 (a) and D8 (b). It should be noted that the two samples are grown with direct and indirect doping methods respectively. It can be seen that the sample surface quality is similar in the two samples.

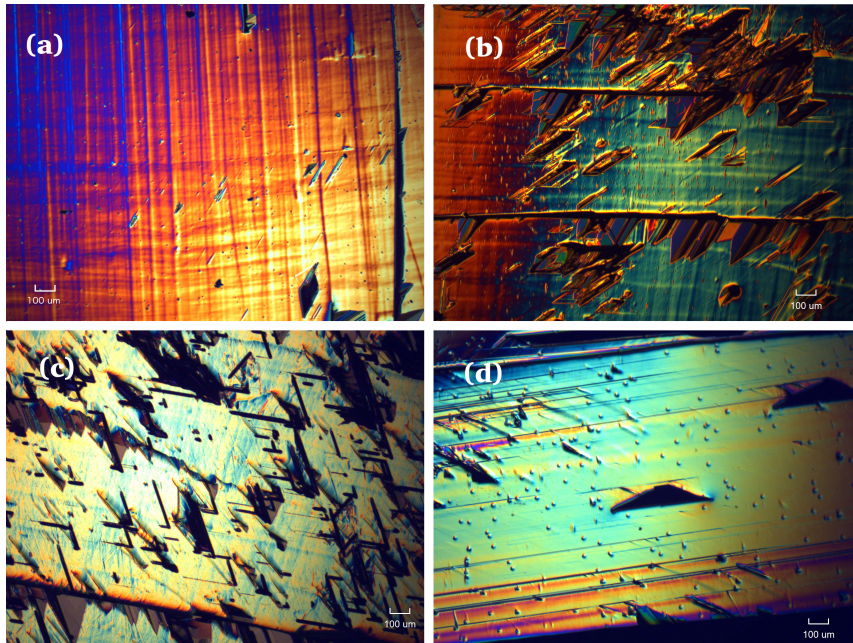


Figure 6.4: Micrographs of an undoped sample (a), doped sample number D1 (b), doped sample number D4 (c) and doped sample number D6 (d).

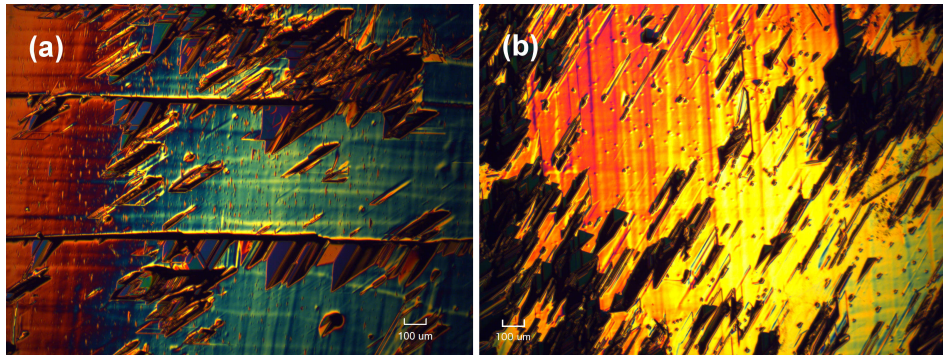


Figure 6.5: Micrographs of samples D1 (a) and D8 (b).

Figure 6.6 shows reflection mode micrographs of samples D6 (a) and D9 (b). These samples are grown with direct and indirect growth methods respectively. Both samples show comparable surface morphology. In (c) a transmission mode micrograph of D9 is shown. It can be seen that there are two different polytypes in the sample. The brighter area in the center is a foreign polytype inclusion.

Absorption measurements were done on directly doped samples with different

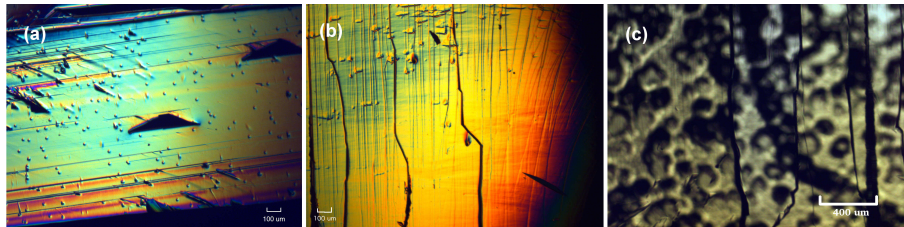


Figure 6.6: Reflection micrographs of samples D6 (a) and D9 (b), and transmission micrograph of D9 (c).

source doping concentrations, samples D1 and D5. The results of these measurements are shown in figure 6.7, together with a reference spectrum from an undoped sample (dotted line). In both samples we see the band edge absorption at around 500 nm. A second feature in the doped sample spectra is the peak at around 700 nm, corresponding to the transition between the boron level and CB. This cannot be seen in the undoped sample. The doped samples show no evidence for a VB to boron transition, which should be seen at around 1800 nm, as described in chapter 2.3. Absorption was also measured for doped samples D6 and D7, but neither the band edge nor the boron related peaks were seen in these highly doped samples.

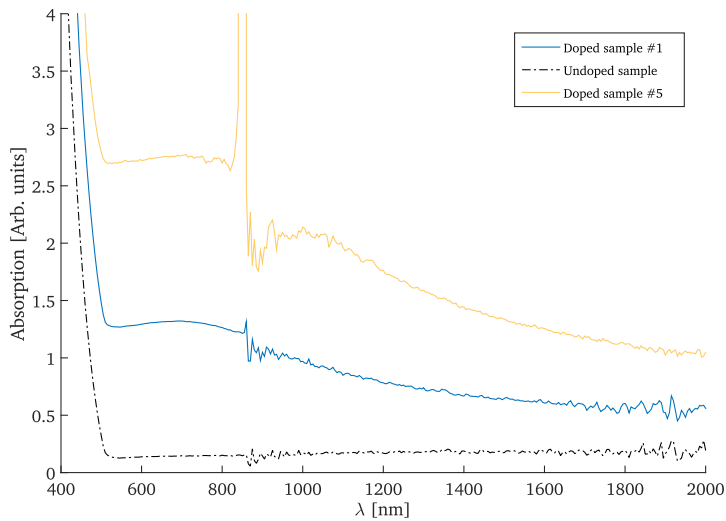


Figure 6.7: Absorption spectrum of undoped sample (dotted line), doped sample D5 (bright yellow line) and doped sample D1 (dark blue line).

Figure 6.8 shows the result of absorption measurements on samples D1 and D8, together with an undoped sample. It should be noted that D8 is an indirectly doped

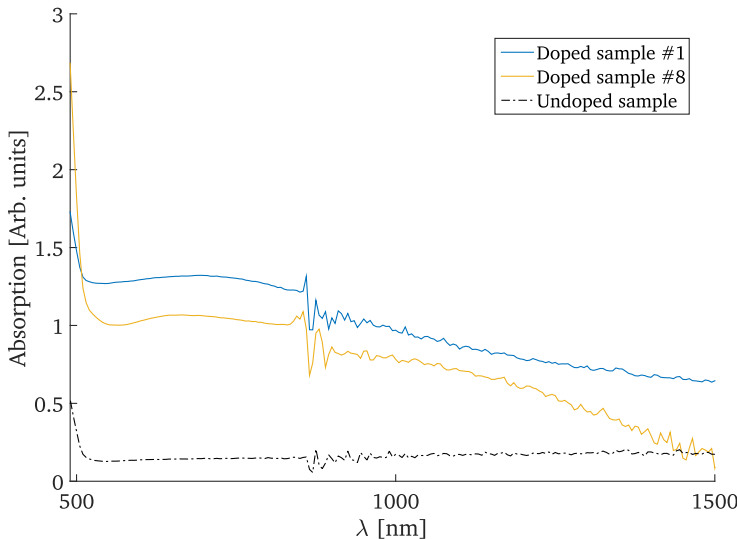


Figure 6.8: Absorption spectrum of doped samples D8 (bright yellow line) and D1 (dark blue line), shown together with an undoped sample (dotted line).

sample. It can be seen that both the doped sample spectra show the same trend. The graphs increase up to a point near the 700 nm B-N transition energy, where they level out. This is not visible in the undoped sample. It can further be seen that sample D8 has its B-N maximum at a slightly shorter wavelength compared to sample D1, which is attributed to the fact that measurements were done on D8 before polishing. The peak shift is in fact a substrate artifact. Absorption measurements were also done on sample D9, which did not show the B-CB peak.

LTPL-measurements were done on boron doped samples and on an undoped seed. Figure 6.9 shows the resulting spectrum of the undoped seed. Five peaks can clearly be seen in the spectrum, labeled as ZPL and phonon replicas. It should be noted that the ZPL is significantly smaller than the phonon replicas. It can further be seen that several smaller peaks appear on the low energy side of the phonon replicas. These lines originate from exciton complexes.

As described in chapter 4.2, the strain in a crystal can be estimated by the fraction between the LA and TO lines. From figure 6.9 this is found to be

$$I_{\text{LA}}/I_{\text{TO}} = 0.783.$$

From the TA-line FWHM, the donor concentration can be found. The FWHM is found to be $\Gamma_{\text{TA}} = 1.094 \text{ meV}$, giving a nitrogen concentration of

$$[N] \approx 10^{16} \text{ cm}^{-3}.$$

This value was obtained by using the same parameters as proposed by Camassel et al. [24].

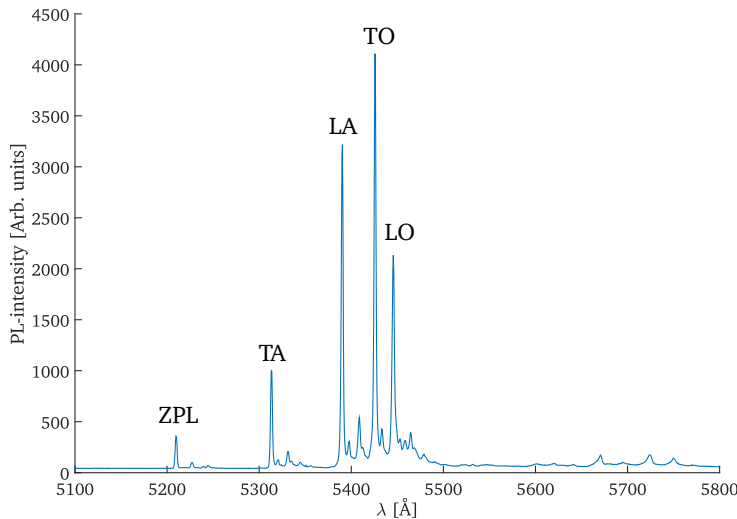


Figure 6.9: LTPL spectrum of an undoped seed. The five main peaks are labeled as ZPL and phonon replicas.

Doped samples D1, D4 and D6 were measured using LTPL. Not one of these samples show any luminescence. Sample D9 did show luminescence from the hexagonal inclusions, but not from the cubic area. The spectrum is shown in figure ??.

<Figure>.

7

Discussion

This chapter discusses the results presented in chapter 6. The chapter is divided into two parts, one part discusses the results of seed growth the other part discusses the results of characterization of the B-doped samples.

7.1 On seed growth

As shown in section 6.1, carbon face grown seeds did not have complete coverage of cubic SiC on the facet, yet the silicon face grown seeds could reproducibly be grown with complete cubic coverage. As seen in figure 3.2, 2D growth is promoted by high supersaturation. A possible explanation of the results is that the supersaturation for the C-face growth was too low. The examined temperatures, as shown in table 6.1 range from 1825 to 1925 °C, which is a large portion of the parameter space in which the 3C-SiC polytype is stable. Changing the temperature much more during growth is unlikely to result in better 3C-coverage, hence the supersaturation will not be able to be changed much more by altering the temperature.

From table 6.1 it can be seen that the percentage of the facet covered by 3C-SiC does not show any trend with regards to temperature. The growth time has been adjusted to get similar sample thickness for all samples. In this way it was possible to only vary the supersaturation between samples. This indicates that for the used growth setup it is not possible to change the supersaturation enough to get complete 3C-SiC coverage of the facet. It should however be mentioned that the pressure conditions for growth have not been explored in this work, and that it may be possible to alter the pressure to get more cubic coverage.

Possible explanations of the difference in 3C-SiC coverage on silicon and carbon face substrates is the spiral growth character. On Si-face the spirals take the form of proper spirals. This gives a structure with steps expanding from the center of the spiral. The C-face spiral takes the form of straight lines extending radially from the

center, as seen in figure 6.1. The 3C-SiC polytype nucleates on top of the heteroepitaxially grown spirals and grows over the spiral steps. The spiral shape can then be expected to influence how the 3C-SiC is grown. The silicon face spiral may be advantageous for cubic growth, while the carbon face spiral may not be.

The silicon and carbon faces have different surface energies, which will influence how material grows on it. This may also be a factor in the problem of growing 3C-SiC on the carbon face. From the micrographs of the carbon face seeds it can be seen that cubic growth always occurs at the edge of the facet, i.e. near the graphite spacer. This is consistent with the hypothesis that the surface energy gives rise to the results, since the edge is expected to have a different surface energy compared to somewhere towards the center of the sample.

7.2 On B-doped samples

From figure 6.4 it can clearly be seen that B-doping deteriorates the crystal quality. All doped samples have a larger number of defects compared to the nominally undoped sample. For samples D1 and D4 the number of defects increase with increasing source doping. This is to be expected, since the boron atoms have a different radius compared to both the silicon and carbon atoms it replaces. This size difference will induce strain in the sample and in turn induce defects. From the same figure we can see that sample D6, which was grown with the source material with the highest doping concentration has smoother surface compared to the two other doped samples. This does not follow the trend. In figure 6.6 (b) can be seen that sample D9, grown from the same source material as D6, shows similarly good surface quality. From the absorption measurements of these samples however, it can be inferred that these materials do not have very good quality. As described in chapter 6, sample D9 does not show any B-CB absorption peak, and D6 does not show the band edge absorption. One possible explanation of this is that the source material does not in fact have the high doping concentration it is thought to have. Another possible explanation is that even though the surface shows a low density of defects, the sample may be of poor crystal quality. This would explain why sample D6 does not show any band edge absorption, which should show even at very low doping concentrations.

Figure 6.5 shows the difference in surface morphology of doped samples D1 and D8, which have been grown using the direct and indirect growth method respectively. The fact that they both show similar numbers of surface defects could indicate that both samples have been doped with comparable concentration of boron. As shown earlier a higher concentration of boron will induce more defects on the surface. Figure 6.8 gives a further indication that this hypothesis is valid. In this figure it can be seen that the two samples give similar absorption spectra. Most importantly both spectra show the B-CB peak at around 700 nm. From this it can be concluded that the indirect doping method introduced in this work is able to introduce impurities in a grown sample. The density of introduced impurities is from the results mentioned here thought to be similar, but methods better suited to give impurity concentrations should be used to validate this finding.

The doped samples D1-D5 and D8 all show band edge absorption and the B-

CB absorption peak, but none of the samples shows the VB-B peak, which should be present at around 1700 nm. A possible explanation for this would be that the B-level is near or below the Fermi level, so that the occupancy of the level is too high to show much absorption. The Fermi level can be computed if the doping concentrations are known. It can be assumed that the nitrogen doping concentration is the same in doped samples as in unintentionally doped samples, i.e. the donor concentration is $N_D \approx 10^{16} \text{ cm}^{-3}$. Assuming that the B-doped samples are of p-type, i.e. $p >> n$, the neutrality condition is

$$p = N_A^- - N_D^+. \quad (7.1)$$

Since the nitrogen energy level is shallow, it can be assumed that at room temperature all donor atoms are ionized. This gives that $N_D^+ = N_D$. Under the Boltzmann approximation the hole density is

$$p \approx N_V e^{-E_F/kT}, \quad (7.2)$$

where N_V is the valence band density of states, and is given by

$$N_V = 2 \left(\frac{k T m_{d,h}}{2 \pi \hbar^2} \right)^{3/2}, \quad (7.3)$$

where $m_{d,h}$ is the density of states hole mass. The number of ionized acceptor atoms is governed by the temperature and the Fermi levels distance from the acceptor level.

$$N_A^- = \frac{N_A}{1 + 2e^{\frac{E_A - E_F}{kT}}}. \quad (7.4)$$

From equations 7.2-7.4 the neutrality condition 7.1 can be rewritten as

$$N_V e^{-E_F/kT} + 2N_V e^{(E_A - 2E_F)/kT} + 2N_D e^{(E_A - E_F)/kT} - N_A + N_D = 0. \quad (7.5)$$

By using the values $E_A = 0.735 \text{ meV}$, $m_{d,h} = 0.6 \times m_0$ and $T = 300 \text{ K}$, equation 7.5 gives the plot in figure 7.1, where the graphs represent N_A concentrations of 10^{17} , 10^{18} and 10^{19} cm^{-3} respectively. It can be seen that for the highest concentration the Fermi level is around 0.57 eV and the highest acceptor concentration gives a Fermi level around 0.70 eV, which is close to the acceptor energy level. From this it can be concluded that for doped samples grown with source impurity concentrations of 10^{18} to 10^{19} cm^{-3} , the Fermi level is below the acceptor energy level, but that there is a significant number of states occupied. This may contribute to the fact that there is no VB-B peak visible in the absorption spectra.

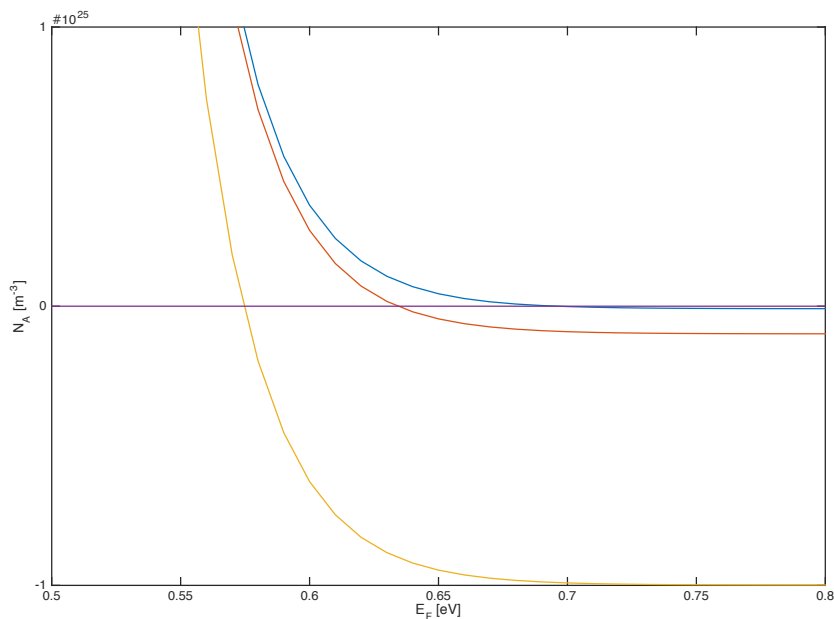


Figure 7.1: Computed values of LHS in equation 7.5, plotted against the Fermi level. The three graphs show acceptor concentrations of 10^{17} , 10^{18} and 10^{19} cm^{-3} .

Outline for PL-discussion

- PL No luminescence from doped cubic. Would suggest that B-level is non-radiative.
Should still show gap luminescence. Maybe crystal quality too poor.
- PL Al luminescence from one doped cubic sample, shows Al inclusions. Possible competition between the impurity types?
- PL High B luminescence from hex inclusion. Why not in cubic? Maybe hexagonal type of B-placement in hex is radiative, but not the cubic placement.
- PL People have shown B luminescence from 3C before. Why not us? High doping -> many defects -> maybe the defects are non radiative?

8

Conclusion

The conclusions drawn from this work are described here.

9

Future work

In this chapter I will write some of my thought of what is to be done in the future concerning these topics.

Bibliography

- [1] E.G. Acheson. Carborundum: Its history, manufacture and uses. *Journal of the Franklin Institute*, 136:279–289, 1893.
- [2] D N Hume and I M Kolthoff. The Silicon Carbide Electrode. *Journal of the American Chemical Society*, 63:2805–2806, 1941.
- [3] R. W. Johnson J. B. Casady. STATUS OF SILICON CARBIDE (SiC) AS A WIDE-BANDGAP SEMICONDUCTOR FOR HIGH-TEMPERATURE APPLICATIONS: A REVIEW. *Solid-State Electronics*, 39(10):1409–1422, 1996.
- [4] Valdas Jokubavicius, G Reza Yazdi, Rickard Liljedahl, Ivan G Ivanov, and Rositsa Yankova. Lateral Enlargement Growth Mechanism of 3C-SiC on Off-Oriented 4H-SiC Substrates. *Crystal growth and design*, 2014.
- [5] B.S. Richards, a. Lambertz, R.P. Corkish, C.a. Zorman, M. Mehregany, M. Ionescu, and M.a. Green. 3C-SiC as a future photovoltaic material. *3rd World Conference on Photovoltaic Energy Conversion, 2003. Proceedings of*, 3:2738–2741, 2003.
- [6] Masashi Kato, Tomonari Yasuda, Keiko Miyake, Masaya Ichimura, and Tomoaki Hatayama. Epitaxial p-type SiC as a self-driven photocathode for water splitting. *International Journal of Hydrogen Energy*, 39(10):4845–4849, March 2014.
- [7] Tomonari Yasuda, Masashi Kato, and Masaya Ichimura. Characterization of Photoelectrochemical Properties of SiC as a Water Splitting Material. *Materials Science Forum*, 717-720:585–588, May 2012.
- [8] Rebecca Cheung. *Silicon Carbide Microelectromechanical Systems Systems for Harsh Environments*. Number February. London, GBR: Imperial College Press, 2006.
- [9] a. P. Mirgorodsky, M. B. Smirnov, E. Abdelmounîm, T. Merle, and P. E. Quintard. Molecular approach to the modeling of elasticity and piezoelectricity of SiC polytypes. *Physical Review B*, 52(6):3993–4000, 1995.
- [10] D. Bimberg, M. Altarelli, and N.O. Lipari. A calculation of valence band masses, exciton and acceptor energies and the ground state properties of the electron-hole liquid in cubic SiC. *Solid State Communications*, 40:437–440, 1981.
- [11] H Aourag, B Djelouli, A Hazzab, and B Khelifa. Pseudopotential calculations on 3C-SiC. *Materials Chemistry and Physics*, 0584(94), 1994.

- [12] Richard Dalven. Temperature coefficient of the energy gap of β -silicon carbide, 1965.
- [13] K Karch, P Pavone, W Windl, O Schütt, and D Strauch. Ab initio calculation of structural and lattice-dynamical properties of silicon carbide. *Physical Review B*, 50(23):17054–17064, 1994.
- [14] J. a. Freitas, S. G. Bishop, P. E. R. Nordquist, and M. L. Gipe. Donor binding energies determined from temperature dependence of photoluminescence spectra in undoped and aluminum-doped beta SiC films. *Applied Physics Letters*, 52(20):1695, 1988.
- [15] Jianwu Sun, Ivan Gueorguiev Ivanov, Rickard Liljedahl, Rositsa Yakimova, and Mikael Syväjärvi. Considerably long carrier lifetimes in high-quality 3C-SiC (111). *Applied physics letters*, 100(252101), 2012.
- [16] Mulpuri V. Rao, J. Tucker, O. W. Holland, N. Papanicolaou, P. H. Chi, J. W. Kretchmer, and M. Ghezzo. Donor ion-implantation doping into SiC. *Journal of Electronic Materials*, 28(3):334–340, 1999.
- [17] P a Ivanov and V E Chelnokov. Recent developments in SiC single-crystal electronics. *Semiconductor Science and Technology*, 7:863–880, 1999.
- [18] Shigehiro Nishino, J. Anthony Powell, and Herbert a. Will. Production of large-area single-crystal wafers of cubic SiC for semiconductor devices. *Applied Physics Letters*, 42(1983):460–462, 1983.
- [19] Hiroyuki Nagasawa, Kuniaki Yagi, and Takamitsu Kawahara. 3C-SiC hetero-epitaxial growth on undulant Si(001) substrate. *Journal of Crystal Growth*, 237-239:1244–1249, 2002.
- [20] J. A. Lely. Darstellung von Einkristallen von Silicium Carbid und Beherrschung von Art und Menge der eingebauten Verunreinigungen. *Berichte der Deutschen Keramischen Gesellschaft*, 32:229–236, 1955.
- [21] H. J. Scheel and T. Fukuda. *Crystal growth technology*. Wiley, 2003.
- [22] Remigijus Vasiliauskas, Maya Marinova, Philip Hens, Peter Wellmann, Mikael Syväjärvi, and Rositsa Yakimova. Nucleation control of cubic silicon carbide on 6H-substrates. *Crystal Growth and Design*, 12:197–204, 2012.
- [23] J. Tauc. Optical properties and electronic structure of amorphous Ge and Si. *Materials Research Bulletin*, 3:37–46, 1968.
- [24] J. Camassel, S. Juillaguet, M. Zielinski, and C. Balloud. Application of LTPL Investigation Methods to CVD-Grown SiC. *Chemical Vapor Deposition*, 12(8-9):549–556, September 2006.

Upphovsrätt

Detta dokument hålls tillgängligt på Internet — eller dess framtida ersättare — under 25 år från publiceringsdatum under förutsättning att inga extraordinära omständigheter uppstår.

Tillgång till dokumentet innebär tillstånd för var och en att läsa, ladda ner, skriva ut enstaka kopior för enskilt bruk och att använda det oförändrat för ickekommersiell forskning och för undervisning. Överföring av upphovsrätten vid en senare tidpunkt kan inte upphäva detta tillstånd. All annan användning av dokumentet kräver upphovsmannens medgivande. För att garantera äktheten, säkerheten och tillgängligheten finns det lösningar av teknisk och administrativ art.

Upphovsmannens ideella rätt innehåller rätt att bli nämnd som upphovsman i den omfattning som god sed kräver vid användning av dokumentet på ovan beskrivna sätt samt skydd mot att dokumentet ändras eller presenteras i sådan form eller i sådant sammanhang som är kränkande för upphovsmannens litterära eller konstnärliga anseende eller egenart.

För ytterligare information om Linköping University Electronic Press se förlagets hemsida <http://www.ep.liu.se/>

Copyright

The publishers will keep this document online on the Internet — or its possible replacement — for a period of 25 years from the date of publication barring exceptional circumstances.

The online availability of the document implies a permanent permission for anyone to read, to download, to print out single copies for his/her own use and to use it unchanged for any non-commercial research and educational purpose. Subsequent transfers of copyright cannot revoke this permission. All other uses of the document are conditional on the consent of the copyright owner. The publisher has taken technical and administrative measures to assure authenticity, security and accessibility.

According to intellectual property law the author has the right to be mentioned when his/her work is accessed as described above and to be protected against infringement.

For additional information about the Linköping University Electronic Press and its procedures for publication and for assurance of document integrity, please refer to its www home page: <http://www.ep.liu.se/>